International Evaluation Co-operation

VOLUME 16

EFFECTS OF SHAPE DIFFERENCES IN THE LEVEL DENSITIES OF THREE FORMALISMS ON CALCULATED CROSS-SECTIONS

*A report by the Working Party
on International Evaluation Co-operation
of the NEA Nuclear Science Committee*

CO-ORDINATOR

C.Y. Fu
Oak Ridge National Laboratory
USA

MONITOR

D.C. Larson
Oak Ridge National Laboratory
USA

NUCLEAR ENERGY AGENCY
ORGANISATION FOR ECONOMIC CO-OPERATION AND DEVELOPMENT

ORGANISATION FOR ECONOMIC CO-OPERATION AND DEVELOPMENT

Pursuant to Article 1 of the Convention signed in Paris on 14th December 1960, and which came into force on 30th September 1961, the Organisation for Economic Co-operation and Development (OECD) shall promote policies designed:

− to achieve the highest sustainable economic growth and employment and a rising standard of living in Member countries, while maintaining financial stability, and thus to contribute to the development of the world economy;
− to contribute to sound economic expansion in Member as well as non-member countries in the process of economic development; and
− to contribute to the expansion of world trade on a multilateral, non-discriminatory basis in accordance with international obligations.

The original Member countries of the OECD are Austria, Belgium, Canada, Denmark, France, Germany, Greece, Iceland, Ireland, Italy, Luxembourg, the Netherlands, Norway, Portugal, Spain, Sweden, Switzerland, Turkey, the United Kingdom and the United States. The following countries became Members subsequently through accession at the dates indicated hereafter; Japan (28th April 1964), Finland (28th January 1969), Australia (7th June 1971), New Zealand (29th May 1973), Mexico (18th May 1994), the Czech Republic (21st December 1995), Hungary (7th May 1996), Poland (22nd November 1996) and the Republic of Korea (12th December 1996). The Commission of the European Communities takes part in the work of the OECD (Article 13 of the OECD Convention).

NUCLEAR ENERGY AGENCY

The OECD Nuclear Energy Agency (NEA) was established on 1st February 1958 under the name of OEEC European Nuclear Energy Agency. It received its present designation on 20th April 1972, when Japan became its first non-European full Member. NEA membership today consist of all OECD Member countries, except New Zealand and Poland. The Commission of the European Communities takes part in the work of the Agency.

The primary objective of the NEA is to promote co-operation among the governments of its participating countries in furthering the development of nuclear power as a safe, environmentally acceptable and economic energy source.

This is achieved by:

− *encouraging harmonization of national regulatory policies and practices, with particular reference to the safety of nuclear installations, protection of man against ionising radiation and preservation of the environment, radioactive waste management, and nuclear third party liability and insurance;*
− *assessing the contribution of nuclear power to the overall energy supply by keeping under review the technical and economic aspects of nuclear power growth and forecasting demand and supply for the different phases of the nuclear fuel cycle;*
− *developing exchanges of scientific and technical information particularly through participation in common services;*
− *setting up international research and development programmes and joint undertakings.*

In these and related tasks, the NEA works in close collaboration with the International Atomic Energy Agency in Vienna, with which it has concluded a Co-operation Agreement, as well as with other international organisations in the nuclear field.

FOREWORD

A Working Party on International Evaluation Co-operation was established under the sponsorship of the OECD/NEA Nuclear Science Committee (NSC) to promote the exchange of information on nuclear data evaluations, validation, and related topics. Its aim is also to provide a framework for co-operative activities between members of the major nuclear data evaluation projects. This includes the possible exchange of scientists in order to encourage co-operation. Requirements for experimental data resulting from this activity are compiled. The Working Party determines common criteria for evaluated nuclear data files with a view to assessing and improving the quality and completeness of evaluated data.

The parties to the project are: ENDF (United States), JEF/EFF (NEA Data Bank Member countries), and JENDL (Japan). Co-operation with evaluation projects of non-OECD countries, specifically the Russian BROND and Chinese CENDL projects, are organised through the Nuclear Data Section of the International Atomic Energy Agency (IAEA).

Subgroup 16 of the Working Party was initiated as a follow-up action to Subgroup 1, which had concluded that many differences in evaluated data files were due to large differences in the level densities used in model calculation. C.Y. Fu was asked to investigate this statement further and to recommend appropriate level densities. The work was started but was, due to unforeseen circumstances, interrupted at an early stage and there were no possibilities to complete the study. The present publication shows the status at the time of the interruption.

Further work on nuclear level densities has been undertaken under the auspices of the IAEA Nuclear Data Section. An example is the Reference Input Parameter Library (RIPL).

The opinions expressed in this report are those of the authors only and do not necessarily represent the position of any Member country or international organisation. This report is published on the responsibility of the Secretary-General of the OECD.

TABLE OF CONTENTS

SUMMARY

Effects of shape differences in the level densities of three formalisms on calculated cross-sections and particle emission spectra are described. Reactions for incident neutrons up to 20 MeV on ^{58}Ni are chosen for illustrations. Level density parameters for one of the formalisms are determined from the available neutron resonance data for one residual nuclide in the binary channels and from fitting the measured (n,n'), (n,p) and (n,α) cross-sections for the other two residual nuclides. Level density parameters for the other two formalisms are determined such that they yield the same values as the above one at two selected energies. This procedure forces the level densities from the three formalisms used for the binary part of the calculation to be as close as possible. The remaining differences are in their energy dependences (shapes). It is shown that these shape differences alone are enough to cause the calculated cross-sections and particle emission spectra to be different by up to 60%.

EFFECTS OF SHAPE DIFFERENCES IN THE LEVEL DENSITIES OF THREE FORMALISMS ON CALCULATED CROSS-SECTIONS

1.   Introduction

The evaluated ^{58}Ni(n,α) cross-sections in the EFF-2 (European), ENDF/B-VI (US) and JENDL-3 (Japanese) libraries are shown in Figure 1. The resolution of the large differences between EFF-2 and ENDF/B-VI was the planned contribution for the first year of this work. It was found that most of these differences are due to factor-of-3 differences in the level densities used in the calculations performed for the evaluations. At the time these evaluations were being carried out, few data were available for this cross-section, hence the heavy dependence on calculation. This part of the work has been reported in detail elsewhere [1] and is summarised in Section 2.

For the second year of the work, the level-density shape differences between Gilbert-Cameron (G-C) [2] and Back-Shifted Fermi Gas (BSFG) [3] were studied via calculated cross-sections and particle emission spectra for ^{58}Ni for incident neutrons up to 20 MeV. Parameters for G-C were taken from the above work and those for BSFG were determined such that the resulting level densities agree with G-C at the top of the discrete level region and near the neutron binding energy for ^{58}Ni, ^{58}Co and ^{55}Fe. This procedure forces the level densities from the two formalisms to be as close as possible for the binary part of the calculation. The remaining differences are in the shapes of the two formalisms that, as shown in Section 3, are capable of causing the calculated cross-sections and particle emission spectra to be different by up to 60%.

For the final year of this work, the Generalised Super-Fluid Model (GSM) [4] was added to the TNG code [5] as a third level-density option. Again the shape effects were studied via ^{58}Ni. However, this time the calculations started with a new evaluation for the s-wave level spacing, D_0, for ^{55}Fe. The Fermi gas parameter a corresponding to this D_0 in the G-C formalism was determined using the G-C pairing correction and a standard formula [4] for the spin cut-off parameter. The parameters for the constant temperature part of G-C were determined automatically in TNG. Since the D_0's for ^{58}Ni and ^{58}Co are not

known experimentally, the corresponding a's in the G-C formalism were found in a series of TNG calculations to fit approximately the (n,n'), (n,p) and (n,α) cross-section data. Several new $^{58}Ni(n,\alpha)$ data sets were taken into account in this fit. The parameters for BSFG and GSM were then obtained by forcing them to agree with G-C at two energies in the same manner as in Section 3 to study the shape effects of the three formalisms. The use of a smaller D_0 for ^{55}Fe resulted in larger values for a for all three residual nuclides, which led to different (n,α) cross-section shapes between G-C and BSFG than those obtained in Section 3. The cross-section ratios and particle-emission spectral rations between GSM and G-C are markedly different from those between BSFG and G-C. This part of work is described in Section 4.

2.   EFF-2 and ENDF/B-VI

It is seen in the evaluated $^{58}Ni(n,\alpha)$ cross-sections shown in Figure 1 that ENDF/B-VI is larger than EFF-2 up to 18 MeV and is about twice as large at 8 MeV. In addition, EFF-2 has a rise-flatten-rise shape not seen in ENDF/B-VI. The resolution of these differences required complete understanding of the formulas and parameters used in the two calculations.

The calculation for EFF-2 was done by Mario Uhl using his MAURINA code [6] and the calculation for ENDF/B-VI was performed by Dave Hetrick with TNG. The two codes use different pre-equilibrium models and different level-density formalisms. Discussion of this problem with Uhl led to the conclusion that one should at first concentrate in the 4 to 12 MeV region where the discrepancy is the largest and where there is a shape change in the cross-sections. In this energy region the pre-equilibrium and tertiary reaction complications can be avoided while the differences in the level-density formalisms are being studied. For these reasons, the present conclusions should be valid only below 12 MeV but the results presented between 12 and 20 MeV are still rather clear and helpful. Because the problems are being solved using the same code, isolation of the effects of each model parameter is possible.

During the presentation of this problem at a NEA/NSC meeting on international evaluation co-operation, Herbert Vonach suggested that using larger level density for the (n,n') channel in Hetrick's calculation would depress the calculated (n,α) cross-section near 8 MeV. This observation is examined quantitatively as described below.

8

Hetrick's calculation was reviewed first. It turned out that his calculated (n,α) cross-sections are 20% larger near 8 MeV than shown in Figure 1. He reduced the calculated results between 6 and 10 MeV to agree with the data measured by Qaim [7]. During this time, Vonach sent information for discrete levels of ^{58}Ni, showing that the level density used for the (n,n') channel in Hetrick's calculation should go higher. This new level scheme was adopted and led to higher level densities between 4 and 10 MeV. This higher level density for the (n,n') channel, however, disrupted the good fits to the (n,n') and (n,p) cross-section data achieved by Hetrick. To restore the good fits, minor adjustments in the level-density parameters for ^{58}Ni and ^{58}Co were made. These adjustments resulted in (n,α) cross-sections slightly smaller than those of ENDF/B-VI shown in Figure 1. So the problem was hardly solved. However, a complete understanding of the TNG calculation was established as a basis for comparison with Uhl's results. The revised calculation is referred to below as Fu's calculation. The new G-C parameters used are listed in Table 1 where U_0 is the G-C pairing correction. The differences between Fu's calculation and Uhl's represent the true calculational differences between ENDF/B-VI and EFF-2 shown in Figure 1.

When Uhl was performing the evaluation, he was not aware of the data of Qaim [7,8] (Figure 1). However, he knew about the 14.8 MeV measurement of Grimes *et al*. [9] (not shown in Figure 1). His calculated (n,α) cross-sections passed through Grimes *et al*. data and were therefore adopted for EFF-2.

All inputs Uhl used in MAURINA were tried in TNG to see if the EFF-2 cross-section shown in Figure 1 could be reproduced. To achieve this, however, the BSFG level-density formalism, used in MAURINA, had to be added to TNG as an option. And a special version of TNG was created to accommodate the energy-dependent radii used in the optical model of MAURINA. Uhl's results as shown in Figure 1 were reproduced to about 10%. The remaining 10% difference could be due to other code differences, such as treatment of widths fluctuations. By testing each model parameter individually, its effect on the calculated (n,α) cross-sections was isolated. The level-density differences in the three binary channels between the two calculations account for about 80% of the (n,α) cross-section differences, as explained in the following paragraph. The differences in the optical-model parameters account for the rest.

The level densities used in Uhl's and Fu's calculations for ^{58}Ni, ^{58}Co and ^{55}Fe are compared as ratios in Figure 2. The BSFG parameters used by Uhl are also listed in Table 1 to compare with the G-C parameters used in Fu's calculation. The symbol δ in Table 1 represents the sum of a pairing correction

and a back energy shift. As shown in Table 2 for incident neutron energy of 8 MeV, more outgoing neutrons and protons reach the level-density regions (continuum) than the corresponding discrete regions, while the alpha particles reach mainly the discrete levels. Higher level densities in ^{58}Ni and ^{58}Co in Uhl's calculation increase the continuum (n,n') and (n,p) cross-sections at the expense of the discrete (n,α) cross-section. This explains the smaller and flattened (n,α) cross-sections in EFF-2 between 6 and 10 MeV. As incident neutron energies go higher than 10 MeV, most outgoing alpha particles begin to see the large ^{55}Fe level densities in Uhl's calculation, and the (n,α) cross-section rises again. Note that the "Uhl calculation" here represents a TNG calculation using all of Uhl's parameters.

The changes in proportions of the discrete and continuum cross-sections between the two calculations seen in Table 2 also cause changes in the particle emission spectra for an incident energy of 8 MeV.

The calculation for JENDL-3 shown in Figure 1 was performed by S. Iijima. Communication with him ended in December 1989 when he died. Therefore, a detailed examination of his calculation was not possible.

During the course of this part of work, it became obvious that there is a large shape difference between the level densities of BSFG and G-C. A first attempt to isolate the effects of these shape differences on calculated cross-sections and particle emission spectra is presented in the next section.

3. Shape differences between BSFG and G-C

For this part of the study, the cross-sections and particle emission spectra in Fu's calculation above were chosen as the G-C reference. This choice is simply a matter of convenience because the numerical results have been stored. A more intelligent choice, leading to higher level densities, is described in Section 4. However, the present results remain interesting, particularly in light of the new results to be presented in Section 4.

The BSFG parameters for each binary residual nuclide were determined by fitting the BSFG level densities to those of G-C at the top of the discrete region, E_c, and the tangent point, E_x, separating the Fermi gas part and the constant temperature part of G-C. The resulting BSFG parameters are listed in Table 1. The level density ratios BSFG/G-C up to 14 MeV are shown in Figure 3. The corresponding particle emission spectra ratios for 14 MeV incident neutrons are shown in Figure 4.

10

The *a* parameters labelled 'BSFG fitted to G-C' are some 16% smaller than those used in Uhl's calculation. For ^{58}Ni and ^{55}Fe, there are increased back shifts. Both factors contribute to the factor-of-3 level density-density ratios labelled Uhl/Fu in Figure 2.

It was decided to adopt E_x instead of the neutron binding energy as one of the fitting energies because E_x is fairly close to the neutron binding energy and has the additional advantage of representing a point of characteristic change in the shape of the G-C level densities. Below E_x, where BSFG level densities are always higher than G-C, the ratios shown in Figure 3 represent the ratios between level densities having a Fermi gas and a constant temperature shape. Above E_x, BSFG and G-C are two Fermi gases with different energy shifts, so must have different *a*'s to yield the same level densities at E_x. In the present case, the *a*'s in BSFG are less than in G-C, so the BSFT/G-C ratios above E_x decrease with increasing excitation energy.

In Figure 4, the neutron, proton and alpha-particle emission ratios above 2 MeV are essentially due to binary reactions and show peaks roughly corresponding to the level density peaks seen in Figure 3, shifted to higher energies for protons and alpha-particles by the respective threshold. The ratios for emitted neutrons less than 2 MeV is smaller than unity because the (n,pn) contribution in BSFG is smaller.

The level density ratios up to 20 MeV and particle emission ratios for 20 MeV incident neutrons are shown respectively in Figures 5 and 6. The differences seen in Figures 3 and 4 are now magnified. The only complication due to tertiary reactions is in the neutron emission ratios for which the peak seen in Figure 4 is missing because the low energy region is filled by tertiary reaction contributions, especially (n,pn).

The (n,α) cross-sections calculated using BSFG and G-C are compared in Figure 7. The agreement is nearly perfect up to 10 MeV, above which the two results start to diverge. There is no rise-flatten-rise shape around 8 MeV in the BSFG calculation because the BSFG level densities are now much lower and the differences between BSFG and G-C are only 10% of those seen in Figure 2. The relative changes between the discrete and continuum cross-sections, listed in Table 2, are rather close to those of the G-C calculation, meaning the particle emission spectra between the two calculations also agree. However, this is only a special case. As shown below in Section 4, the rise-flatten-rise shape in BSFG re-appears when a set of larger level densities is used.

The (n,α) cross-sections in Figure 7 show that BSFG at 20 MeV is 60% larger than G-C. In the BSFG calculation at this energy, most outgoing alpha particles see larger level densities than outgoing neutrons and protons do (see Figure 5) because of the higher Coulomb energy and lower thresholds for alpha particle emission.

The importance of the level density problem on theoretical computation of (n,α) cross-sections and alpha particle emission spectra is now well established. But many questions remain. In the following, a more thorough investigation is carried out which, as pointed out in the concluding remarks, is still inadequate to fully clear up the problems associated with G-C, BSFG and GSM.

4. Additional analyses and inclusion of GSM

A new calculation for the ^{58}Ni cross-sections was made (1) to account for a new evaluation of s-wave level spacing D_0 for ^{55}Fe, (2) to account for the measured (n,α) cross-sections and (3) to get a better set of G-C level density parameters for ^{58}Ni, ^{58}Co and ^{55}Fe that yield reasonable agreement with the available (n,n'), (n,p) and (n,α) cross-section data, to begin the investigation with.

4.1 D_0 for ^{55}Fe

Among the level densities required for calculating the binary cross-sections, the only measured D_0 available is for ^{55}Fe. This D_0 value was fixed at 14.4 keV (20.4 keV in the G-C calculations above) based on the recent analysis of Zhao and Su [10]. The Fermi gas parameter a in G-C was derived from D_0 using:

$$U = E - U_0, U = at^2, \sigma^2 = \left(6/\pi^2\right)a\left\langle m^2\right\rangle t, \left\langle m^2\right\rangle = 0.24A^{2/3}$$

where E is the excitation energy and U_0 is the pairing energy correction, taken here as 1.54 MeV.

In the TNG code, the required input for G-C are a, $\left\langle m^2\right\rangle$ and U_0 for the Fermi gas part. The parameters for the constant temperature part of G-C (energy shift E_0, temperature T and tangential point E_x) are determined automatically in TNG from the input for the Fermi gas part and the discrete levels. The energy of the highest discrete level is called E_c. If $\left\langle m^2\right\rangle$ is not given, TNG takes the

formula above as default. So in the calculations using G-C, the necessary input are a and U_0 while the adjustable one to fit cross-sections is normally only a.

The effective excitation energy U is defined differently in the BSFG and the GSM formulas to be given below.

4.2 Fit to ^{58}Ni cross-sections

The a values for ^{58}Ni and ^{58}Co were adjusted via a series of TNG calculations to fit (n,n'), (n,p) and (n,α) cross-sections using G-C. Since no other model parameters were adjusted, the fit is not optimal. However, it is important to note that once the a value for ^{55}Fe is fixed, there can only be one set of a's possible in the fit.

The resulting G-C parameters are shown in Table 3, where the BSFG and GSM parameters described below are also listed for comparison.

The resulting cross-sections are shown in Figure 8. Experimental cross-sections are not shown, but it is sufficient for the present purpose to note that the calculated values agree with 'evaluated' data to about 10%.

4.3 BSFG versus G-C

The BSFG a and the shift Δ for each of the binary residual nuclides are obtained by fitting the BSFG level densities to G-C determined above at E_c and E_x. The resulting BSFG parameters can also be found in Table 3.

The BSFG/G-C ratios up to 20 MeV are shown in Figure 9. Note each E_x is now smaller and closer, compared to that in Figure 5, to the neutron binding energy due to the use of a larger a. This set of smaller E_x drops the BSFG/G-C ratios above E_x some more. The relative changes in the BSFG/G-C ratios among the three residual nuclides are different and result in different changes in the cross-sections.

The spin cut-off factor in BSFG used here is given by:

$$\sigma^2 = 0.0150 A^{5/3} t, U - \Delta = at^2 - t$$

13

The effects of this different spin cut-off factor on cross-sections and particle emission spectra have been determined to be much smaller than the shape effects being addressed in this report.

The effects of the level-density shape differences between BSFG and G-C on cross-sections are shown in Figure 10 and on particle emission spectra for an incident energy of 20 MeV are shown in Figure 11.

From Figure 10, it is seen that the BSFG/G-C ratios for (n,α) have a valley between 4 and 12 MeV. This means the rise-flatten-rise shape in EFF-2 seen in Figure 1 but not seen in Figure 7 re-appears. This phenomenon cannot be explained by comparing the differences in the BSFG/G-C ratios shown in Figures 5 and 9. The explanation can be found from the larger a's used here that increase the continuum parts, relative to the discrete parts, of all cross-sections (Table 4). Since the (n,n') and (n,p) cross-sections at 8 MeV have much larger continuum components than (n,α), the preference for neutron and proton emission due to the larger BSFG level densities are magnified. For incident energies greater than 12 MeV, the outgoing alphas in the BSFG calculation begin to see larger BSFG level densities than the outgoing neutrons and protons do, so the BSFG (n,α) gets larger.

The particle emission spectra ratios shown in Figure 11 have the same behaviour as shown above in Figure 6. For example, neutron emission below 4 MeV for BSFG is larger because the BSFG (n,pn), the dominant low-energy neutron emitter, is larger. And neutron emission around 10 MeV for BSFG is reduced because the BSFG (n,n') cross-section is reduced.

In summary, the present set of larger a's yields a different shape in the BSFG (n,α) cross-sections but the same shapes in the particle emission spectra compared to a lower set of a's used in Section 3.

4.4 GSM versus G-C

The GSM asymptotic a and the shift δ for each of the binary residual nuclides are obtained by fitting GSM level densities to G-C determined above at E_c and E_x.

The resulting GSM/G-C level density ratios are shown in Figure 12. These ratios are closer to unity than BSFG/G-C ratios shown in Figure 9, due to the energy-dependent Fermi gas parameters that increase with increasing excitation

14

energy. However, the differences in cross-sections and particle emission spectra between GSM and G-C are larger than between BSFG and G-C, as discussed below. The GSM parameters are also listed in Table 3. Values of the shell corrections needed for GSM were obtained from the HERMES code of Mengoni [11].

Note that the spin cut-off factor in GSM is the same as used above for G-C, but U is defined differently:

$$U = E - E_{cond} + n\Delta_0 + \delta, \Delta_0 = 12A^{-1/2}$$

where A is the mass number, $n = 0,1,2$ for even-even, odd-A and odd-odd nuclide. E_{cond} is the condensation energy in the model calculated from other input parameters. E_{cond}-$n\Delta_0$ is the pairing correction. The effects of the level density shape differences between GSM and G-C on cross-sections are shown in Figure 13 and on particle emission spectra for an incident energy of 20 MeV are shown in Figure 14. The super-fluid region has no impact here because this region lies below E_c.

From Figure 13, it is seen that the GSM/G-C ratios for (n,α) have a maximum at 8 MeV instead of a minimum seen in Figure 10. This new behaviour can be explained by comparing the level density ratios of Figures 9 and 12 and, at the same time, looking at the GSM distributions of discrete and continuum cross-sections listed in Table 4. While for an incident neutron energy of 8 MeV all GSM level densities are greater than G-C, the distribution between the discrete and continuum cross-sections have changed. The outgoing neutrons and protons in GSM see fewer continuum levels, resulting in smaller (n,n′) and (n,p) continuum cross-sections and larger (n,α) discrete and continuum cross-sections. In other words, the 8 MeV maximum in the GSM/G-C is more a result of redistribution of cross-section within the GSM calculation itself than a difference between the level densities of GSM and G-C. For incident energies greater than 12 MeV, the GSM level densities clearly favour the (n,n′) cross-sections.

The shapes of the GSM/G-C ratios for particle emission shown in Figure 14 are reversed from those of BSFG/G-C shown in Figure 11. For example, neutrons emitted below 4 MeV in the GSM calculation are lower because the GSM (n,pn) cross-sections are smaller. And neutron emissions for GSM around 10 MeV are higher due to larger GSM (n,n′) cross-sections.

Even though the GSM/G-C ratios are closer to unity than BSFG/G-C, the differences between calculated GSM and G-C cross-sections and particle emission spectra are larger due to the larger relative changes in level densities among the three residual nuclides. For example, between 10 and 20 MeV, BSFG/G-C ratios in Figure 9 move down with energy but stay parallel. This fact changes the particle emission spectra more than the cross-sections. On the other hand and in the same energy range, the GSM/G-C ratios in Figure 12 also decrease with energy but do not stay parallel. This new behaviour changes the cross-sections more and changes the particle emission spectra by an even larger amount because the differences in cross-sections also show up in the emission spectra.

5. Concluding remarks

It is now clear that, given a nucleus with an adequate number of discrete levels and neutron resonance data, the three level density formalisms studied in this report would give different level densities at all excitation energies other than at the top of the discrete level region and the neutron binding energy. The resulting calculated cross-sections, particularly (n,α), and particle emission spectra would also be different by up to 60%. In less ideal situations where little or no experimental level density data exist, the calculated (n,α) cross-sections can differ by a factor of two due to the additional uncertainty in the level density parameters.

In this section, tentative remarks, based on theoretical consideration, on the strengths and weaknesses of each level density model studied in this report are offered for the sake of stimulating wider research in this important area.

The fact that G-C has a constant temperature part for low excitation energies and a Fermi gas part for higher energies is a strength, not a weakness as is generally perceived [3,4], at least for the present calculations. First, the number of discrete levels in each residual nuclide required in the present calculations defines the level density at E_c rather well. Therefore the constant temperature part of G-C requires no input parameters. Second, the Fermi gas part used to fit the experimental D_0 value is not disrupted by an arbitrary energy shift (other than the pairing energy shift) that has no physical meaning in the Fermi gas model. The original argument by G-C for introducing the constant temperature part is to compensate for the low-energy collective levels not included in the Fermi gas model.

16

The weakness of G-C is in its shell correction that is included in a constant a for all excitation energies. At high excitation energies, in which particles far below the Fermi surface get excited, the shell correction should diminish. This dwindling shell correction is treated in GSM, one of its strengths.

GSM has the strongest physics in both pairing corrections and shell corrections. However, the fact that GSM still needs an arbitrary energy shift δ to fit both D_0 at the neutron binding energy and the level density in the discrete level region, at least for ^{55}Fe considered here, is a disappointment. It is seen from Figure 12 that GSM/G-C is smaller than unity above E_x. This means the effects of the shift factor overpower the effects of the dwindling shell corrections. In case the shift factor is small, such as for ^{116}Sn in Ref. 4, the basic physics intended for GSM is maintained.

For similar reasons, the back shift Δ used in BSFG has no physical basis. Like G-C, the shell corrections in BSFG are accounted for in a constant a determined at the neutron binding energy, a second weakness.

As tentative recommendations, BSFG should be restricted to calculations at low energies, perhaps lower than 14 MeV. G-C may be used to much higher energies if shell corrections are small. For example, G-C should not be used for the Pb isotopes, probably not above 10 MeV, because of large shell corrections. GSM is not widely understood and deserves more applications to clear up any possible problems. In case the shift factor used in GSM is large, as in the present calculations for ^{58}Ni, the effects of the shift tend to overpower the intended physics built in the super-fluid pairing model and the energy dependent shell correction. And the required input of shell corrections for GSM from different sources [11,12] may be different.

REFERENCES

[1] C.Y. Fu, D.C. Larson, D.M. Hetrick, H. Vonach, J. Kopecky, S. Iijima, Y. Yamamuro, T. Asami, S. Chiba, G. Maino, I. Mengoni, "Report of Subgroup 1 of the NEA/NSC Working Party on International Evaluation Co-operation", NEA/WPEC-1.

[2] A. Gilbert and A.G.W. Cameron, *Can. J. Phys*. 13, 1446 (1965).

[3] W. Dilg, W. Schantl, H. Vonach and M. Uhl, *Nucl. Phys*. A217, 269 (1973).

[4] A.V. Ignatyuk, J.L. Weil, S. Raman and S. Kahane, *Phys. Rev*. C47, 1504 (1993).

[5] K. Shibata and C.Y. Fu, "Recent Improvements of the TNG Statistical Model Code", ORNL/TM-10093 (1986), and C.Y. Fu, " A Consistent Nuclear Model for Compound and Precompound Reaction Cross-Section Calculations", ORNL/TM-7042 (1980).

[6] M. Uhl, Institute of Radiation and Nuclear Physics, University of Vienna, Vienna, Austria, private communication (1990).

[7] S.M. Qaim, R. Wolfe, N.M. Rahman, *Nucl. Sci. Eng*. 88, 143 (1984).

[8] S.M. Qaim and N.I. Molla, *Nucl. Phys*. A283, 269 (1977).

[9] S.M. Grimes *et al*., *Phys. Rev*. C19, 2127 (1979).

[10] Z. Zhao and Z. Su, Chinese Nuclear Data Center, private communication (1994).

[11] A. Mengoni and Y. Nakajima, *J. Nucl. Sci. Tech*. 31, 151 (1994) and private communication (1995).

[12] A. Zelenetsky, Institute of Atomic Energetics, Obninsk, Russia, private communication (1995).

Table 1. Level density parameters for Figures 2 and 3

		^{58}Ni	^{58}Co	^{55}Fe
Gilbert-Cameron				
Fu's calculation				
G-C (Fu)	a	5.400	6.200	5.909
For Figures 2 and 3	U	2.470	0	1.540
Back-Shifted Fermi Gas				
Uhl's calculation	a	5.517	6.061	5.821
For Figure 2	δ	0.104	-2.571	-0.700
BSFG fitted to G-C (Fu)				
at E_c and E_x	a	4.600	5.260	5.000
For Figure 3	δ	-0.500	-2.600	-1.100

Table 2. Discrete and continuum parts of ^{58}Ni
cross-sections (mb) for an incident energy of 8 MeV
calculated using level density parameters of Table 1*

	Discrete			Continuum		
	(n,n')	(n,p)	(n,α)	(n,n')	(n,p)	(n,α)
G-C (Fu)	341	181	72.2	536	391	11.2
BS (Uhl-TNG)	217	42	37.9	612	502	16.2
BS fitted to G-C	344	176	70.9	528	400	12.9

* *This table corresponds to Figure 7. All model parameters other than level densities were chosen for and stayed fixed throughout this paper.*

Table 3. Level density parameters for Figures 9 and 12

		^{58}Ni	^{58}Co	^{55}Fe
Gilbert-Cameron	a	6.200	7.300	7.256
For Figures 9 and 12	U	2.470	0	1.540
Back-Shifted Fermi Gas	a	5.332	6.210	6.188
For Figure 9	δ	0.210	-1.910	-0.210
Generalised Super-Fluid Model				
For Figure 12	asymptotic a	6.496	7.266	7.576
	δ	2.680	1.468	1.530
	shell corr.	-4.037	-2.318	-2.977

**Table 4. Discrete and continuum parts of ^{58}Ni
cross-sections (mb) for an incident energy of 8 MeV
calculated using level density parameters of Table 3***

	Discrete			Continuum		
	(n,n')	(n,p)	(n,α)	(n,n')	(n,p)	(n,α)
G-C	296	144	57.7	580	444	12.1
BS fitted to G-C	265	114	45.4	628	471	12.7
GSM fitted to G-C	371	171	69.3	503	395	17.2

** This table corresponds to Figures 8, 10 and 13. All model parameters other than level densities
were chosen for and stayed fixed throughout this paper.*

Figure 1. Evaluated ^{58}Ni(n,α) cross-sections in ENDF/B-VI, JENDL-3 and EFF-2. ENDF/B-VI at 8 MeV is twice as large as EFF-2, and EFF-2 has a rise-flatten-rise shape not seen in the other two evaluations. The data shown are due to Qaim *et al.* [7,8].
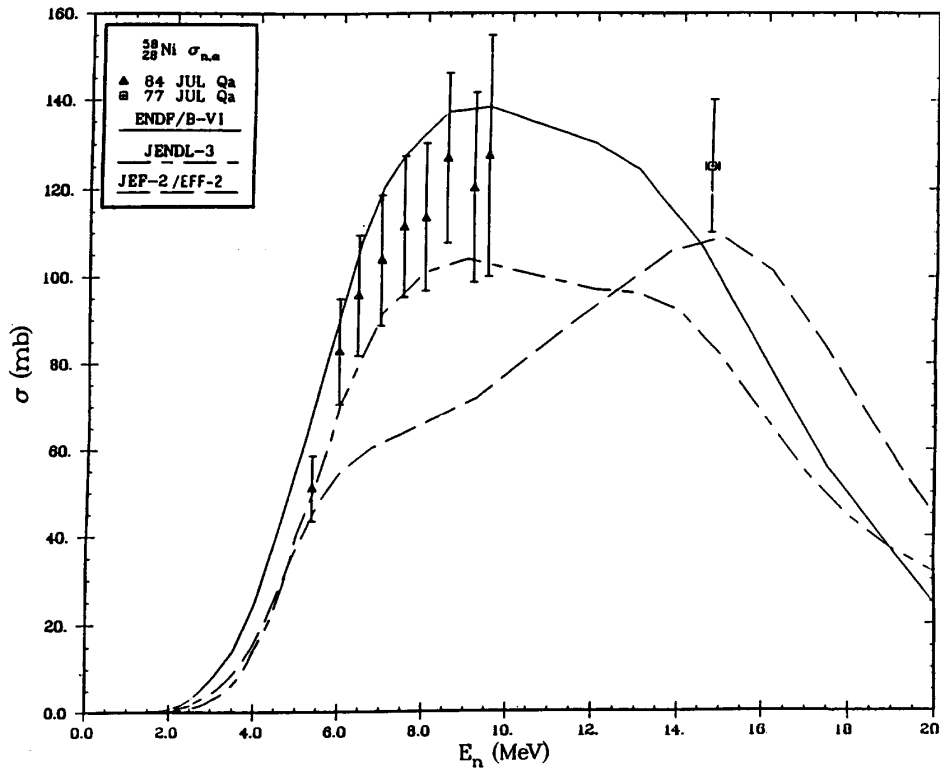
Figure 2. Level densities used in Uhl's calculation for EFF-2 and in Fu's calculation (approximately representing ENDF/B-VI in Figure 1) are compared as ratios for three residual nuclides in the binary reactions of neutrons with ^{58}Ni. These level-density differences account for about 80% of the differences between the calculated ^{58}Ni(n,α) cross-sections for ENDF/B-VI and EFF 2.
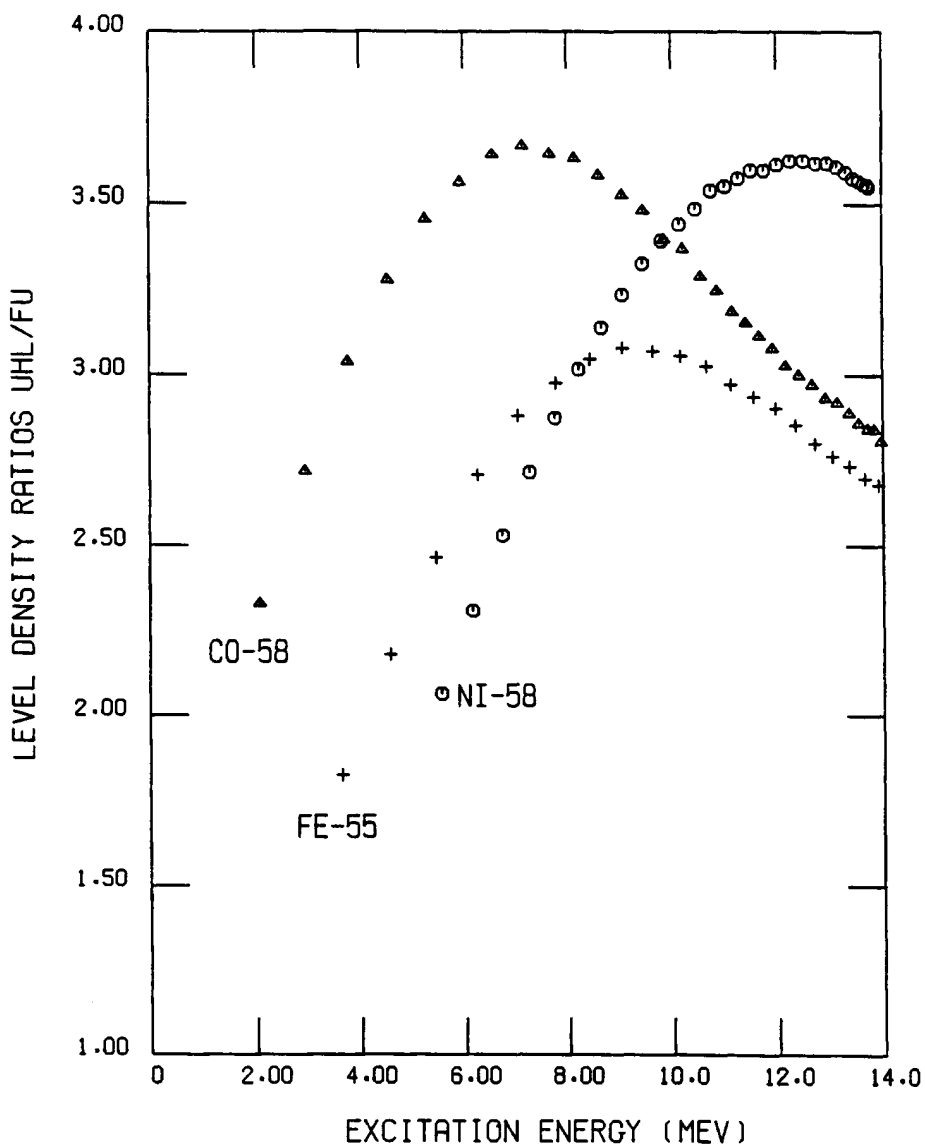
Figure 3. Parameters of the BSFG formalism are determined by fitting its level densities at two energies, E_c and E_x, to G-C used in Fu's calculation shown in Figure 2. The resulting level densities are compared as ratios for three residual nuclides in the binary reactions of neutrons with ^{58}Ni.

25
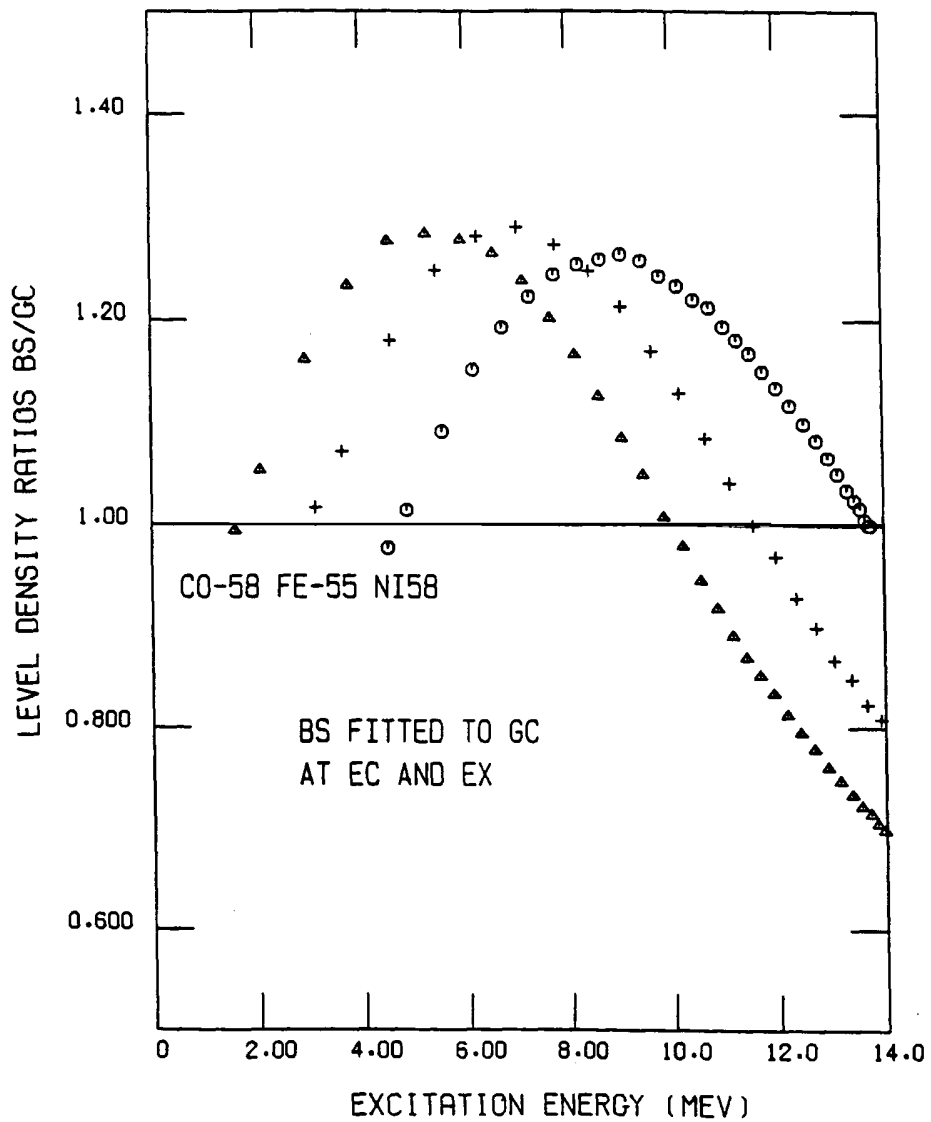
Figure 4. Neutron, proton and alpha particle emission spectra for an incident neutron energy of 14 MeV calculated using the BSFG and G-C level densities indicated in Figure 3 are compared as ratios. The peaks in these ratios correspond to the peaks in the level-density ratios shown in Figure 3, shifted by the respective reaction threshold.
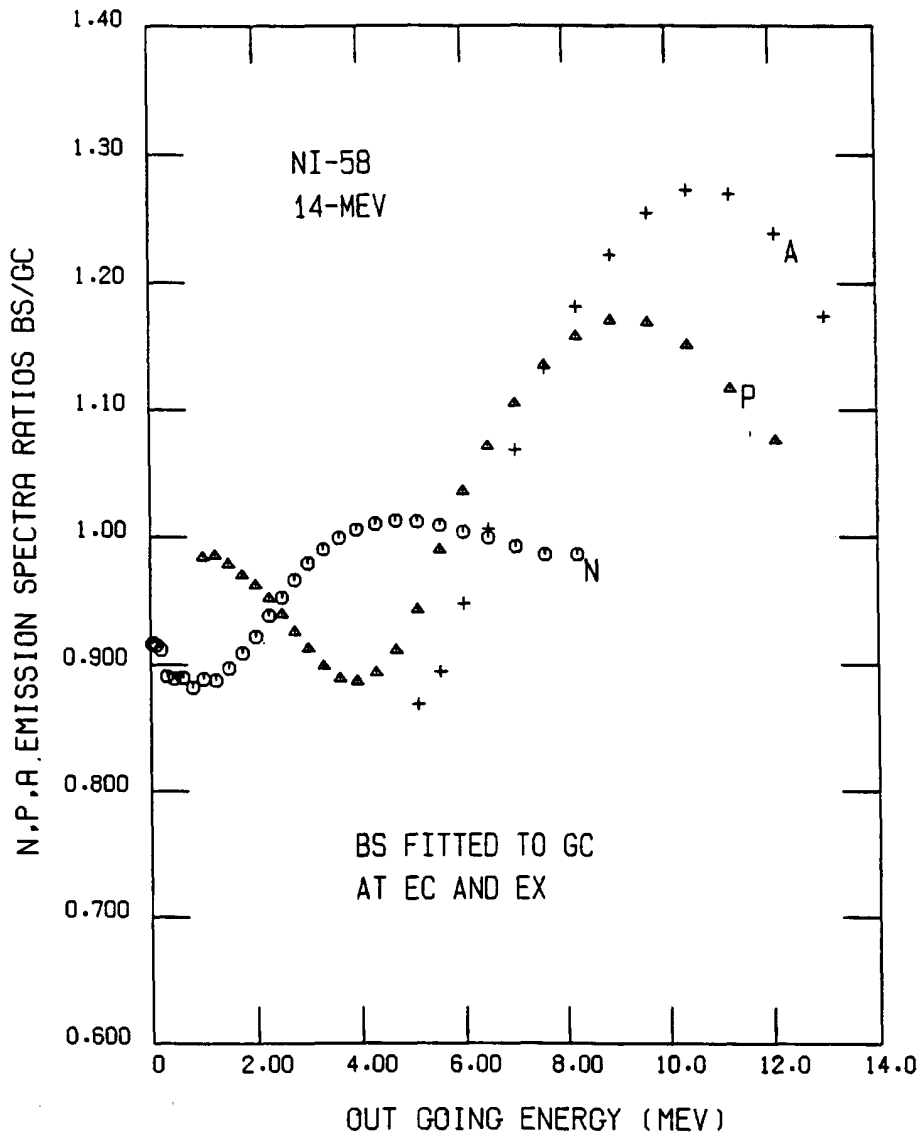
Figure 5. Same as Figure 3 but extended to higher excitation energies. The difference between BSFG and G-C level densities for each residual nuclide increases as the excitation energy increases above E_x.
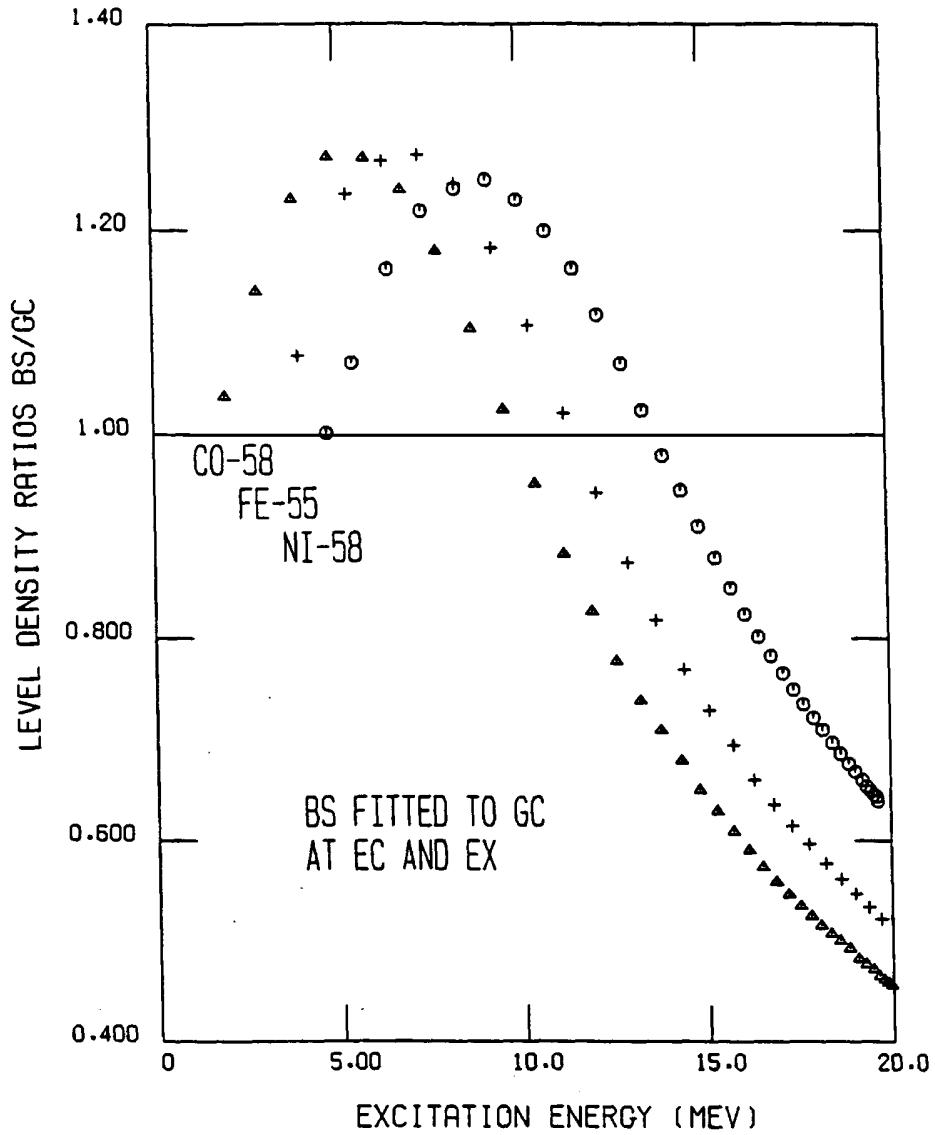
Figure 6. Same as Figure 4 but for an outgoing energy of 20 MeV. The differences between the calculated spectra are magnified, particularly for alpha particles, from those for 14 MeV.
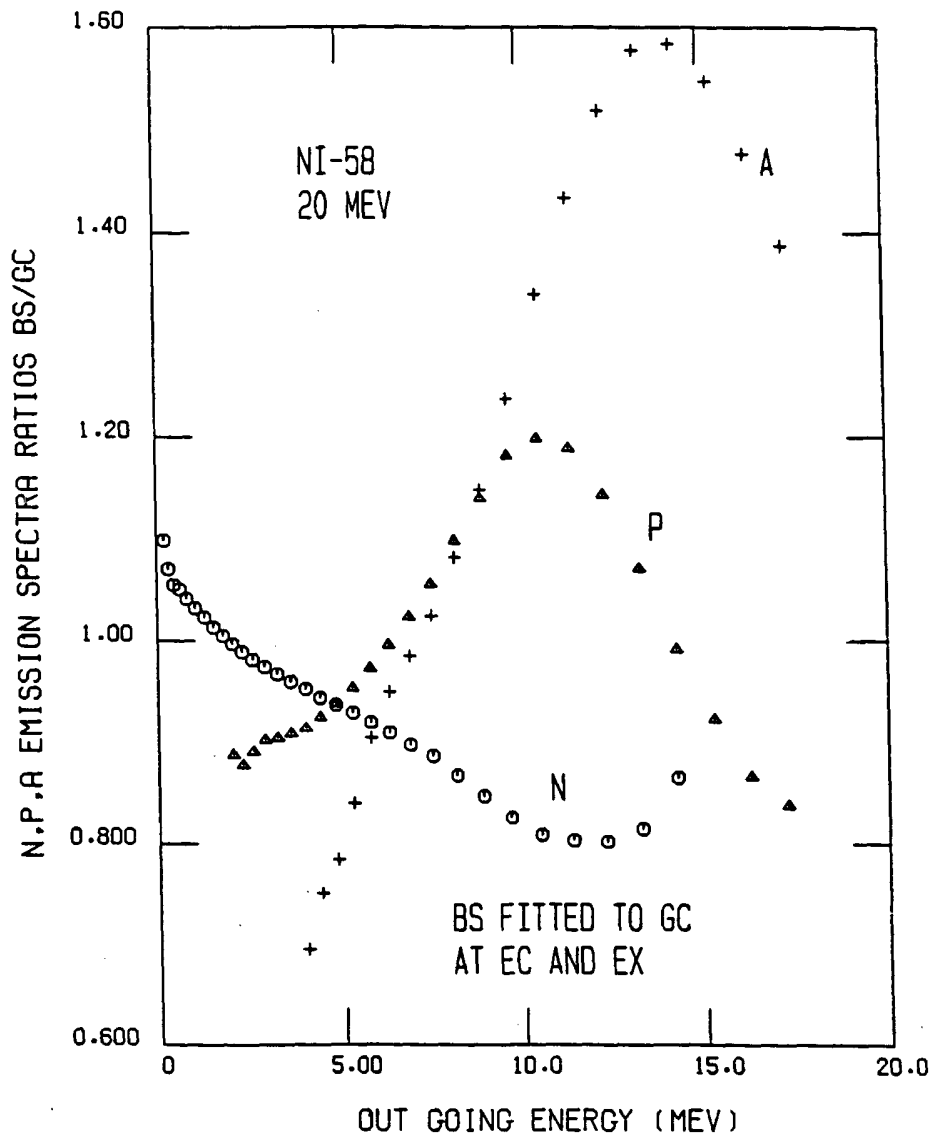
Figure 7. The ^{58}Ni(n,α) cross-sections calculated using BSFG and G-C shown in Figure 5 are compared. At 20 MeV, BSFG is 60% larger than G-C. In BSFG calculation at this incident energy, most outgoing alpha particles see larger level densities than outgoing neutrons and protons do because of the higher Coulomb energy and lower threshold for alpha particle emission.
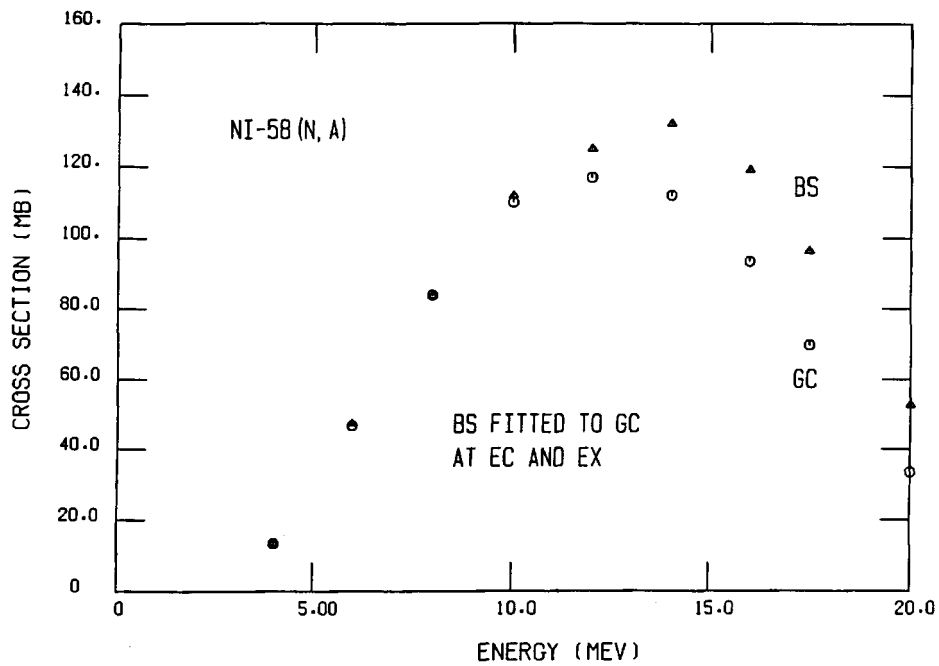
Figure 8. ^{58}Ni(n,n'), (n,p) and (n,α) cross-sections calculated using recommended level densities for the (n,α) channel and adjusted level densities for the (n,n') and (n,p) channels fitting the measured cross-sections. This figure is presented as a basis for comparisons below.
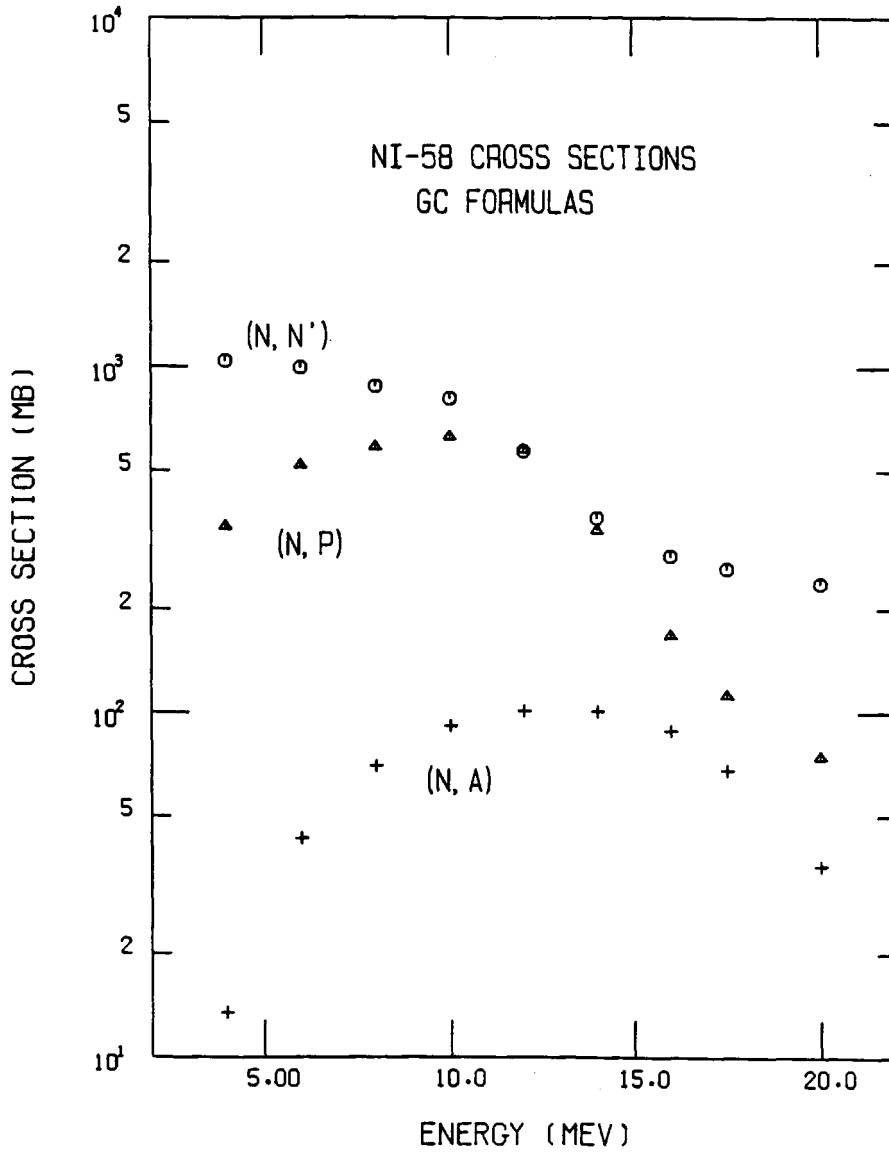
Figure 9. Same as Figure 5 except for a different set of level-density parameters obtained from the calculations shown in Figure 8. Note the following differences from Figure 5: the peak in ^{55}Fe ratios is lower, the E_x's are lower, the high-energy tails move down more and the ^{55}Fe tail moves closer to ^{58}Co.
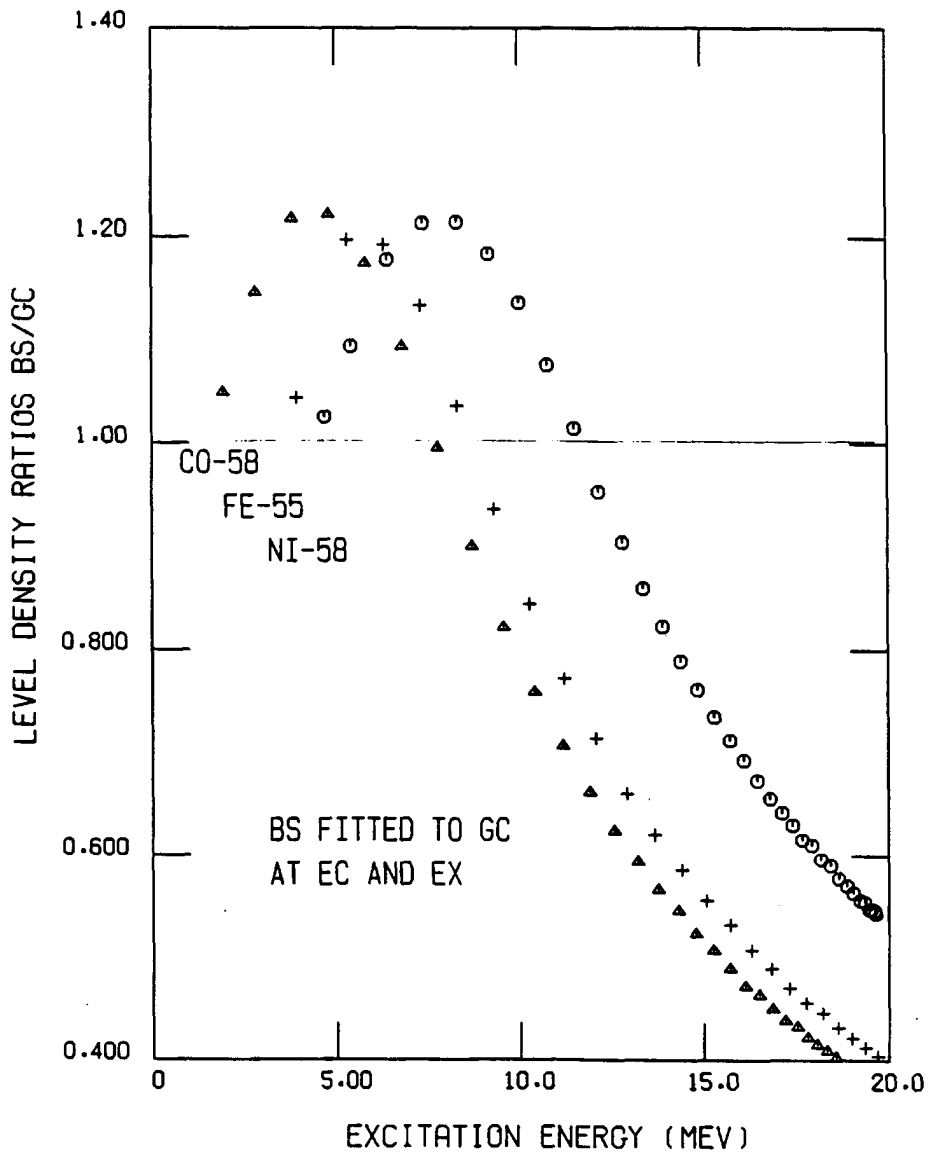
Figure 10. The ^{58}Ni(n,n'), (n,p) and (n,α) cross-sections calculated using the BSFG and G-C level densities compared in Figure 9 are compared as ratios. The minimum in (n,α) at 8 MeV indicates that the rise-flatten-rise shape seen in Figure 1 but not in Figure 7 re-appears. *See text for explanation.*
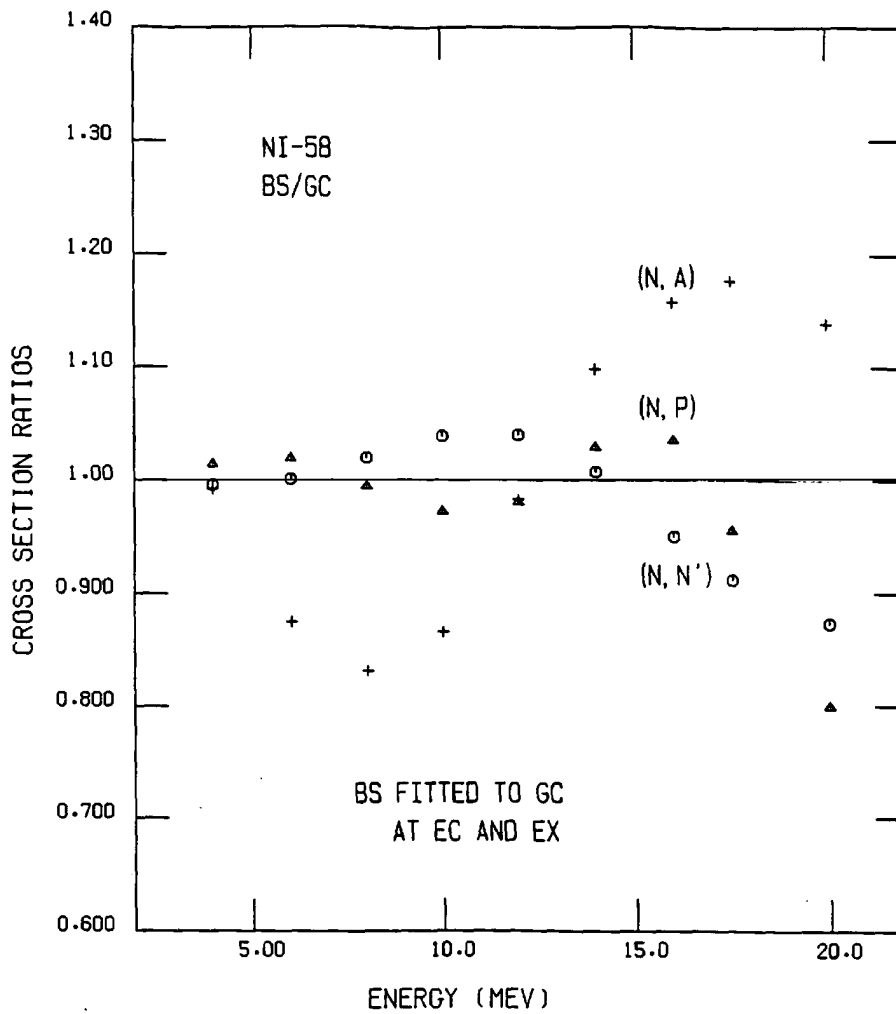
Figure 11. Same as Figure 6 except for a different set of level density parameters obtained from the calculations shown in Figure 8. The peak in the alpha particle emission ratios is now lower because the ^{55}Fe tail shown in Figure 9 is lower.
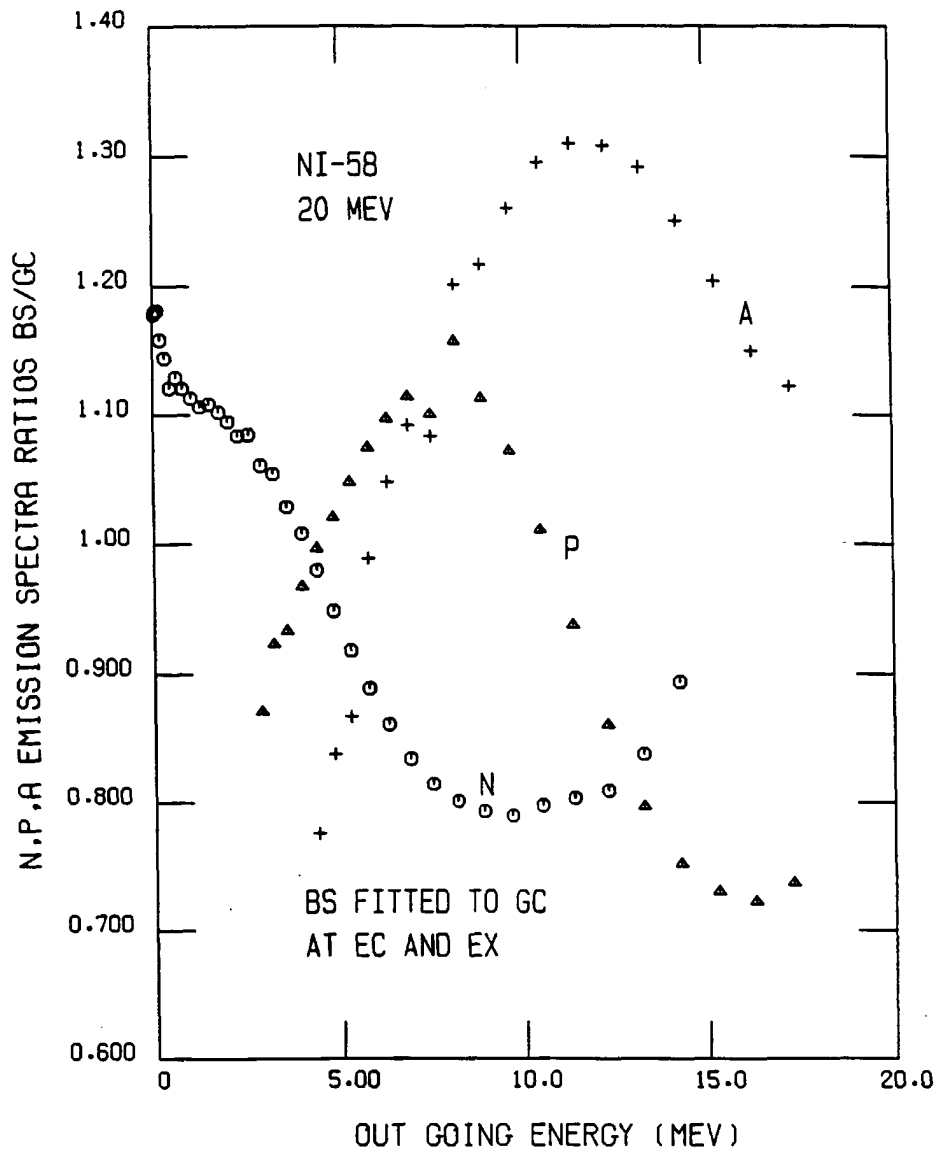
Figure 12. Parameters of the GSM formalism are determined by fitting its level densities at two energies, E_c and E_x, to G-C used in the calculation shown in Figure 8. The resulting level densities in GSM and G-C are compared as ratios for three residual nuclides in the binary reactions of neutrons with ^{58}Ni. Relative to the BSFG/G-C ratios shown in Figure 9, the present ratios are closer to unity but have different shapes for the three residual nuclides.
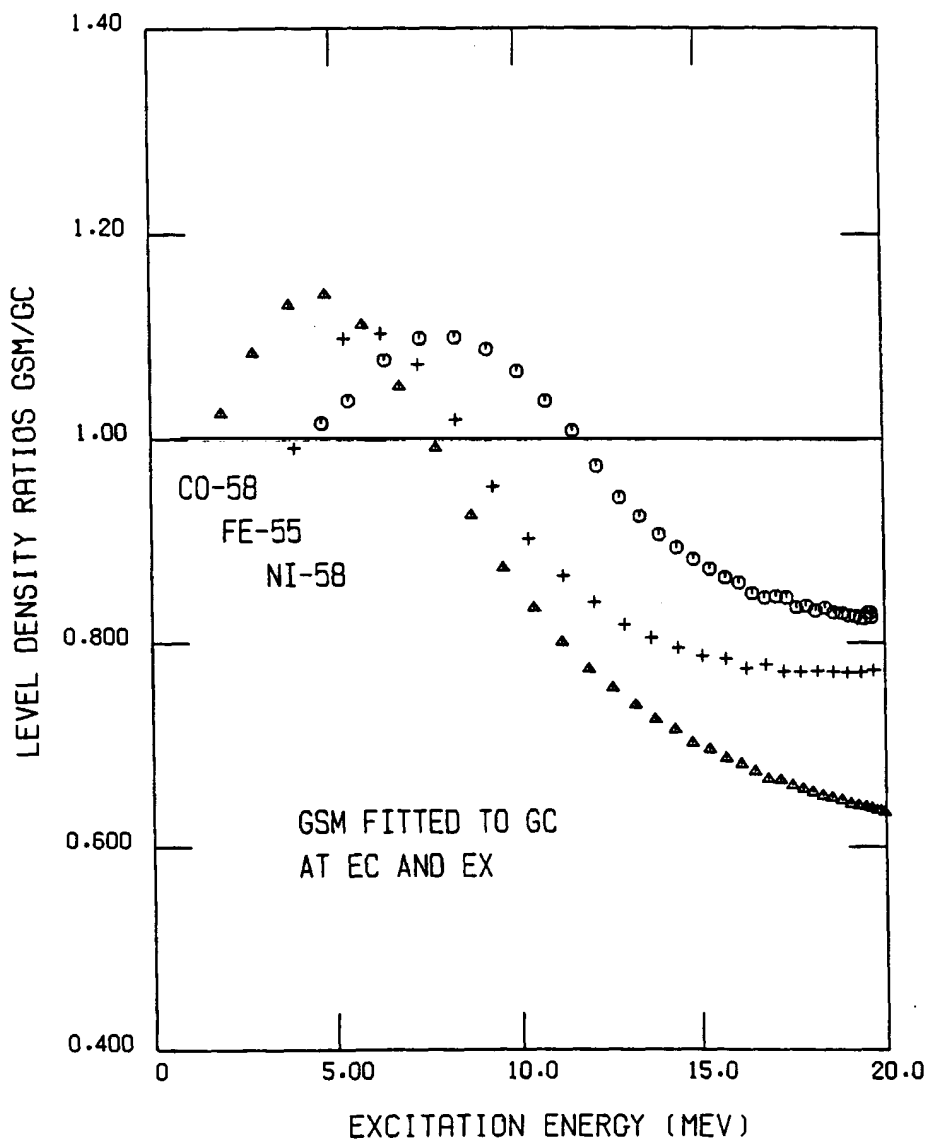
Figure 13. The ^{58}Ni(n,n'), (n,p) and (n,α) cross-sections calculated using the GSM and G-C level densities indicated in Figure 12 are compared as ratios. Comparing with the corresponding BSFG/G-C ratios shown in Figure 10, the (n,α) ratio at 8 MeV appears as a maximum instead of a minimum and the high-energy (n,n') ratios instead of (n,α) are larger. *See text for explanation.*
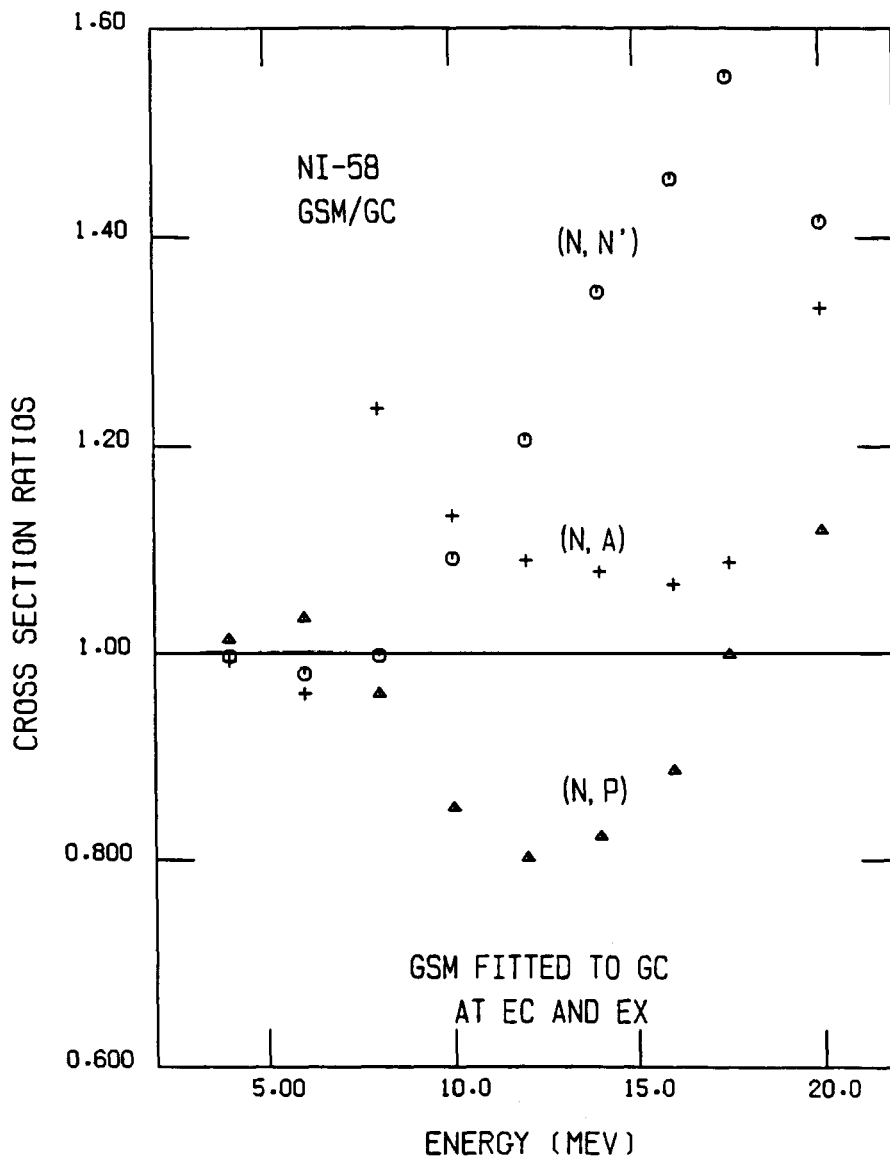
Figure 14. Neutron, proton and alpha particle emission spectra for an incident neutron energy of 20 MeV calculated using the GSM and G-C level densities indicated in Figure 12 are compared as ratios. These ratios behave differently from those for BSFG/G-C shown in Figure 11 because both the level density ratios shown in Figure 12 and the cross-section ratios shown in Figure 13 have new characteristics.